crystals

MDPI

Article

Formation of Tetranuclear Nickel(II) Complexes with Schiff-Bases: Crystal Structures and Magnetic Properties

Zhonglu You [1], Yingying Luo [1], Susan Herringer [2], Yanmin Li [1], Silvio Decurtins [2], Karl W. Krämer [2] and Shi-Xia Liu [2,*]

[1] Department of Chemistry and Chemical Engineering, Liaoning Normal University, Dalian 116029, China; youzhonglu@innu.edu.cn (Z.Y.); ying19950819@126.com (Y.L.); liyanmin940919@126.com (Y.L.)

[2] Departement für Chemie und Biochemie, Universität Bern, Freiestrasse 3, CH-3012 Bern, Switzerland; susan.herringer@dcb.unibe.ch (S.H.); decurtins@dcb.unibe.ch (S.D.); karl.kraemer@dcb.unibe.ch (K.W.K.)

* Correspondence: liu@dcb.unibe.ch; Tel.: +41-31-631-3397

Received: 19 June 2020; Accepted: 6 July 2020; Published: 9 July 2020

Abstract: The cubane-type structure is a typical representative of tetranuclear coordination compounds. In this work, two anionic Schiff-base ligands, $(L^1)^{2-}$ and $(L^2)^{2-}$, each offering an OˆNˆO coordination pocket, ligate four Ni^{II} ions into a $[Ni_4O_4]$ cubane core. The ligands are H_2L^1 = 2−[[(3-ethoxy-2−hydroxyphenyl) methylene]amino]benzenemethanol and H_2L^2 = 2−[[(5-fluoro-2−hydroxyphenyl)methylene]amino]benzenemethanol. In both compounds, $[Ni_4(L^1)_4(EtOH)_4]$ (**1**) and $[Ni_4(L^2)_4(MeOH)_4]$ (**2**), alkoxy oxygens of the ligands act in a bridging μ_3-O binding mode. Magnetic susceptibility and magnetization data for compounds **1** and **2** are presented. The Ni–O–Ni bond angles of the cubane core determined from single crystal X-ray diffraction data play a key role for a magneto-structural correlation. Dominant intracube ferromagnetic behavior is observed, and the coupling parameters were determined for both compounds, leading to nonzero spin ground states in accordance with the broadly accepted bond angle guideline.

Keywords: Cubane-type structure; magnetic properties; nickel cluster; Schiff-base; structure elucidation

1. Introduction

In the field of polynuclear coordination chemistry, skillful design strategies involving polytopic ligands often lead to predictable cluster structures, in which bridged transition metal ions exhibit appreciable magnetic spin–spin exchange [1–7]. Advantageously, such polynucleating ligands comprise coordination pockets, by which the spin centers are bound in adjacent pairs favoring intramolecular spin communication. Amongst the most versatile and widely studied ligand systems for the design of cluster compounds are polydentate Schiff-bases incorporating for the most part O/N donor atoms [8–21]. Due to the ease of access of Schiff-bases and their flexible structures, highly versatile cluster compounds with a broad variety of structure types can be realized. One prominent class of compounds shows a cubane-type structure containing four metal ions and four ligand O-donor atoms at the corners of a cube; each of the subsets forms a tetrahedron [22–30]. The compact cubane core with its specific bonding pattern allows for strong magnetic couplings between the spin centers, but also for a rich redox chemistry of the whole unit. For the latter, attention has recently been attracted for testing these tetrametallic molecular systems in applications as water oxidation catalysts [31–33] or for electrocatalytic methanol oxidation reactions [34]. In the field of molecular magnetism, cubane-like clusters have for long been in the center of magnetic studies [8–19,22–30,35–40], while deliberately and systematically looking for magnetostructural correlations. Thereby, one can note that even slight structural rearrangements of the cubane core, e.g., caused by exchange of coordinated solvent or loss

of lattice solvent can lead to drastic changes of the magnetic properties. As a matter of facts, for Ni^{II} cubane structures, a clear correlation between the Ni–O–Ni bond angles formed via triply-bridged oxygen atoms and the magnetic coupling strengths is observed [23,40–43]. For angles above 99°, the magnetic coupling between the Ni^{II} ions is antiferromagnetic, but ferromagnetic for smaller angles. To note, structural distortions may affect this kind of guideline.

In this paper, we report the synthesis, characterization, and magnetic properties of two cubane-type complexes with stoichiometries $[Ni_4(L^1)_4(EtOH)_4]$ (**1**) and $[Ni_4(L^2)_4(MeOH)_4]$ (**2**), both based on anionic Schiff-base ligands $(L^1)^{2-}$ and $(L^2)^{2-}$, respectively (Figure 1). The magnetic susceptibility and magnetization data were determined, and the former were fitted based on a Heisenberg Hamiltonian with two different coupling parameters J_1 and J_2 in the case of **1**, and with one J parameter for **2**. Both compounds are found to be in a ferromagnetic coupling regime, in agreement with their structural parameters.

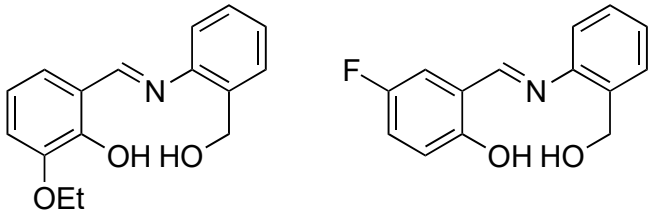

Figure 1. Chemical Structures of the Ligands H_2L^1 (left) and H_2L^{2-} (right); the doubly deprotonated ligands bind to the Ni^{II} ions of the cluster cores.

2. Materials and Methods

2.1. Materials

3-Ethoxysalicylaldehyde, 5-fluorosalicylaldehyde, and 2−aminobenzylalcohol were purchased from Sigma Aldrich, USA. Nickel acetate tetrahydrate and solvents employed for the syntheses were of analytical grade and used as received without further purification.

2.2. General Methods

Elemental analyses were performed on a 240C elemental analyzer (Perkin-Elmer, USA). IR spectra were recorded on an FT/IR-4000 spectrometer (Jasco, Japan) as KBr pellets in 4000–400 cm^{-1} region. UV-vis spectra were recorded on a Lambda 35 spectrometer (Perkin-Elmer, USA). ^1H and ^{13}C NMR spectra were recorded on a 500 MHz spectrometer (Bruker, Germany). Single crystal X-ray diffraction was carried out on an Apex II CCD area diffractometer (Bruker, Germany). Powder X-ray diffraction patterns were measured on a StadiP diffractometer (STOE, Darmstadt, Germany) in Debye Scherrer geometry.

2.3. Synthesis of Ligands and Complexes

2.3.1. Synthesis of H_2L^1

Similar to the previously reported procedure [44,45], 3-ethoxysalicylaldehyde (1.66 g, 0.01 mol) was rected with 2−aminobenzylalcohol (1.23 g, 0.01 mol) in methanol (30 mL). The mixture was stirred at room temperature for 1 h to give a yellow solution, which was evaporated by distillation to give a yellow solid product. The solid was recrystallized from methanol to give the crystalline product H_2L^1. Yield: 92%. Elemental analysis (%) calcd for $C_{16}H_{17}NO_3$: C, 70.83; H, 6.32; N, 5.16; found: C, 70.67; H, 6.44; N, 5.0. IR data (KBr, cm^{-1}): 3528 (OH), 1612 (C=N), 1570, 1456, 1384, 1245, 1186, 1105, 1038, 988, 900, 858, 782, 735. UV-vis data (λ, ε): 226 nm, 1.67×10^4 $L{\cdot}mol^{-1}{\cdot}cm^{-1}$; 278 nm, 9.75×10^3 $L{\cdot}mol^{-1}{\cdot}cm^{-1}$; 317 nm, 8.93×10^3 $L{\cdot}mol^{-1}{\cdot}cm^{-1}$. ^1H NMR (500 MHz, d^6-DMSO): δ 13.26 (s, 1H, O*H*), 8.87 (s, 1H, C*H*=N), 7.54 (t, 1H, Ar*H*), 7.36-7.31 (m, 3H, Ar*H*), 7.24 (d, 1H, Ar*H*), 7.12 (d, 1H, Ar*H*), 6.90

(t, 1H, Ar*H*), 5.19 (t, 1H, O*H*), 4.65 (d, 2H, CH_2OH), 4.08 (q, 2H, OCH_2CH$_3$), 1.36 (t, 3H, OCH$_2$CH_3). ^{13}C NMR (126 MHz, DMSO) δ 163.36, 150.85, 147.03, 145.35, 135.77, 127.81, 127.37, 126.64, 124.08, 119.40, 118.48, 117.73, 116.89, 64.06, 59.39, 14.73.

2.3.2. Synthesis of H_2L^2

5-Fluorosalicylaldehyde (1.40 g, 0.01 mol) was reacted with 2−aminobenzylalcohol (1.23 g, 0.01 mol) in methanol (30 mL). The mixture was stirred at room temperature for 1 h to give a yellow solution, which was evaporated by distillation to give a yellow solid product. The solid was recrystallized from methanol to give the crystalline product H_2L^2. Yield: 94%. Elemental analysis (%) calcd for $C_{14}H_{12}FNO_2$: C, 68.56; H, 4.93; N, 5.71; found: C, 68.71; H, 5.02; N, 5.63. IR data (KBr, cm^{-1}): 3338 (OH), 3246, 1620 (C=N), 1565, 1481, 1354, 1255, 1197, 1138, 1028, 957, 867, 778. UV-vis data (λ, ε): 230 nm, 1.81×10^4 L·mol^{-1}·cm^{-1}; 265 nm, 1.30×10^4 L·mol^{-1}·cm^{-1}; 347 nm, 1.17×10^4 L·mol^{-1}·cm^{-1}. ^{1}H NMR (500 MHz, d^6-DMSO): δ 12.70 (s, 1H, O*H*), 8.84 (s, 1H, C*H*=N), 7.54 (s, 1H, Ar*H*), 7.38-7.28 (m, 3H, Ar*H*), 7.02 (m, 2H, Ar*H*), 6.90 (t, 1H, Ar*H*), 5.19 (t, 1H, O*H*), 4.78 (d, 2H, CH_2OH). ^{13}C NMR (126 MHz, DMSO) δ 162.25, 156.96, 156.35, 151.51, 136.39, 128.37, 127.97, 120.79, 120.53, 120.24, 120.18, 118.27, 115.81, 59.88.

2.3.3. Synthesis of [Ni$_4$(L^1)$_4$(EtOH)$_4$] (**1**)

H_2L^1 (27.1 mg, 0.1 mmol) was reacted with nickel acetate tetrahydrate (24.9 mg, 0.1 mmol) in ethanol (20 mL). The mixture was stirred at room temperature for 30 min to give a green solution, which was allowed to stand in air for a few days until three quarter of the solvent was evaporated. Green block-shaped single crystals of the complex were formed at the bottom of the vessel. The crystals were isolated by filtration and dried in air. Yield: 27%. Elemental analysis (%) calcd for $C_{72}H_{84}N_4Ni_4O_{16}$: C, 57.80; H, 5.66; N, 3.74; found: C, 57.65; H, 5.72; N, 3.67. IR data (KBr, cm^{-1}): 1606 (C=N), 1541, 1443, 1389, 1331, 1230, 1183, 1108, 1045, 740, 620, 565, 525, 461. UV-vis data (λ, ε): 243 nm, 1.56×10^4 L·mol^{-1}·cm^{-1}; 310 nm, 6.91×10^3 L·mol^{-1}·cm^{-1}; 415 nm, 3.79×10^3 L·mol^{-1}·cm^{-1}; 577 nm, 5.10×10^2 L·mol^{-1}·cm^{-1}.

2.3.4. Synthesis of [Ni$_4$(L^2)$_4$(MeOH)$_4$] (**2**)

H_2L^2 (24.5 mg, 0.1 mmol) was reacted with nickel acetate tetrahydrate (24.9 mg, 0.1 mmol) in methanol (20 mL). The mixture was stirred at room temperature for 30 min to give a green solution, which was allowed to stand in air for a few days until three quarter of the solvent was evaporated. Green block-shaped single crystals of the complex were formed at the bottom of the vessel. The crystals were isolated by filtration and dried in air. Yield: 23%. Elemental analysis (%) calcd for $C_{60}H_{56}F_4N_4Ni_4O_{12}$: C, 53.95; H, 4.23; N, 4.19; found: C, 54.14; H, 4.30; N, 4.31. IR data (KBr, cm^{-1}): 1608 (C=N), 1538, 1463, 1386, 1313, 1243, 1192, 1135, 1043, 873, 815, 751, 620, 525, 457. UV-vis data (λ, ε): 241 nm, 1.68×10^4 L·mol^{-1}·cm^{-1}; 300 nm, 8.30×10^3 L·mol^{-1}·cm^{-1}; 420 nm, 7.49×10^3 L·mol^{-1}·cm^{-1}; 575 nm, 3.71×10^2 L·mol^{-1}·cm^{-1}.

2.4. X-ray Crystallography

Diffraction intensities for the complexes were collected at 298(2) K using a Bruker Apex II CCD area-detector diffractometer with MoKα radiation (λ = 0.71073 Å). Collected data were reduced with SAINT [46], and multiscan absorption correction was performed using SADABS [47]. Structures of the complexes were solved by direct methods and refined against F^2 by full-matrix least-squares method using SHELXTL [48]. All nonhydrogen atoms were refined anisotropically. The hydrogen atoms were placed in calculated positions and constrained to ride on their parent atoms. The ethanol ligand C36-C35-O8 of **1** is disordered over two sites, with occupancies of 0.385(2) and 0.615(2). Crystallographic data for the complexes are summarized in Table 1. Selected Ni-L bond lengths and Ni–O–Ni angles of **1** are given in Table 2. Further L-Ni-L and Ni–O–Ni angles of **2** are reported in Supplementary Materials Table S1.

CCDC 1946462 (**1**) and 1946463 (**2**) contain the supplementary crystallographic data for this paper. These data can be obtained free of charge from the Cambridge Crystallographic Data Center, 12 Union Road, Cambridge CB2 1EZ, UK; Fax: (+44)1223-336-033; or E-mail: deposit@ccdc.cam.ac.uk.

Table 1. Details of the data collection and refinement parameters for complexes **1** and **2**.

	1	**2**
Empirical formula	$C_{72}H_{84}N_4Ni_4O_{16}$	$C_{60}H_{56}F_4N_4Ni_4O_{12}$
Formula weight/g mol^{-1}	1496.27	1335.93
Crystal shape/colour	block/green	block/green
Crystal size/mm	0.15 × 0.13 × 0.12	0.11 × 0.10 × 0.07
Crystal system	Monoclinic	Monoclinic
Space group	*C*2/*c*	$P2_1/n$
a (Å)	21.4621(12)	14.8500(13)
b (Å)	14.9753(11)	15.0271(11)
c (Å)	21.9416(13)	27.5089(17)
β (°)	91.826(1)	97.873(1)
V (Å^3)	7048.5(8)	6080.8(8)
Z	4	4
μ (Mo*Kα*) (cm^{-1})	1.121	1.295
T_{min}	0.8498	0.8707
T_{max}	0.8772	0.9148
Reflections/parameters	20581/454	35744/761
Unique reflections	6554	11296
Observed reflections [$I \geq 2\sigma(I)$]	3916	6171
Restraints	7	0
Goodness of fit on F^2	0.984	1.014
R_1, wR_2 [$I \geq 2\sigma(I)$]	0.0469, 0.1027	0.0658, 0.1734
R_1, wR_2 (all data)	0.0970, 0.1282	0.1322, 0.2174

Table 2. Selected bond lengths (Å) and angles (°) for complexes **1** and **2**.

1			
Ni1–O1	1.972(3)	Ni1–O2	2.002(2)
Ni1–N1	2.049(3)	Ni1–O5	2.092(3)
Ni1–O2′	2.093(3)	Ni1–O8	2.171(3)
Ni2–O4	1.975(3)	Ni2–O5	2.003(3)
Ni2–N2	2.056(4)	Ni2–O5′	2.095(2)
Ni2–O2′	2.100(3)	Ni2–O7	2.143(3)
Ni1–O2–Ni1′	101.56(10)	Ni1′–O5–Ni2	95.20(10)
Ni1–O2–Ni2	97.82(11)	Ni1′–O5–Ni2	97.62(11)
Ni1–O2′–Ni2′	94.63(10)	Ni2–O5–Ni2′	101.53(10)
2			
Ni1–O1	1.971(5)	Ni1–O2	1.994(4)
Ni1–N1	2.047(6)	Ni1–O4	2.099(4)
Ni1–O6	2.114(4)	Ni1–O9	2.153(5)
Ni2–O3	1.971(4)	Ni2–O4	1.999(4)
Ni2–N2	2.050(5)	Ni2–O8	2.085(4)
Ni2–O2	2.093(4)	Ni2–O10	2.158(5)
Ni3–O5	1.973(5)	Ni3–O6	2.001(4)
Ni3–N3	2.060(6)	Ni3–O8	2.102(4)
Ni3–O4	2.102(4)	Ni3–O11	2.182(5)
Ni4–O7	1.970(4)	Ni4–O8	1.995(4)
Ni4–N4	2.049(5)	Ni4–O6	2.086(4)
Ni4–O2	2.099(4)	Ni4–O12	2.166(5)
Ni1–O2–Ni2	100.6(2)	Ni1–O2–Ni4	98.6(2)
Ni1–O4–Ni2	100.3(2)	Ni2–O2–Ni4	94.5(2)
Ni1-O4-Ni3	96.0(2)	Ni2–O4–Ni3	98.3(2)
Ni1–O6–Ni3	98.7(2)	Ni3–O6–Ni4	100.3(2)
Ni1–O6–Ni4	95.3(2)	Ni2–O8–Ni3	95.7(2)
Ni3–O8–Ni4	99.9(2)	Ni2–O8–Ni4	97.8(2)

3. Results and Discussion

3.1. Synthesis and Characterization

The Schiff-bases H_2L^1 and H_2L^2 were readily prepared by the condensation reaction of 2−aminobenzylalcohol with 3-ethoxysalicylaldehyde and 5-fluorosalicylaldehyde, respectively, in methanol. The nickel complexes **1** and **2** were prepared by the reaction of nickel acetate tetrahydrate with H_2L^1 in ethanol, and with H_2L^2 in methanol, respectively. Consequently, ethanol and methanol molecules were found as terminal ligands in the coordination environment of **1** and **2**, respectively (*vide infra*).

The infrared spectra of the complexes and the free Schiff-bases were recorded in the region 4000–400 cm^{-1}. The intense absorption bands at 1606–1608 cm^{-1} in the spectra of the complexes are assigned to the imine stretching frequency of the Schiff-base ligands [49]. The shift of the bands to lower frequency, compared to the free Schiff-bases (1612–1620 cm^{-1}), indicates the coordination of the imine nitrogen atom to the Ni^{II} ion [49,50]. The phenolic ν_{Ar-O} in the free Schiff-bases exhibits strong bands at 1245–1255 cm^{-1}, whereas these bands are observed in the lower frequency region at 1183–1192 cm^{-1} in the complexes, indicating the coordination to the nickel atoms through the phenolate oxygen atoms [51]. The Schiff-base coordination to the nickel atoms is substantiated by prominent bands appearing at low wave numbers of 450-620 cm^{-1}, which can be attributed to ν(Ni–N) and ν(Ni–O) [52].

The UV-vis absorption bands observed around 415–420 nm can be attributed to the transition from the coordinated Schiff-base ligands to the nickel atoms (LMCT) [53]. The bands centered at 241–243 and 300–310 nm may be assigned to the intraligand π-π^* and n-π^* transitions, respectively [54]. The broad low-intensity absorption bands centered at 570-580 nm are typical *d-d* bands for the nickel atoms [55].

3.2. Structural Description of the Complexes

Compounds **1** and **2** crystallize in the monoclinic space groups $C2/c$ and $P2_1/n$, respectively, and their molecular structures are shown in Figure 2. Both clusters present analogous stoichiometries, namely, $[Ni_4(L^1)_4(EtOH)_4]$ for **1** and $[Ni_4(L^2)_4(MeOH)_4]$ for **2**, and they reveal the same structural architecture and binding configuration of their ligands. Therefore, the structural description is focused on compound **1**. Its main element consists in a $[Ni_4O_4]$ cubane core, which resides on a crystallographic two-fold rotation axis. The Ni^{II} ions are connected by alkoxy oxygens from four anionic Schiff-base ligands $(L^1)^{2-}$ exhibiting four μ_3-O binding modes. It is worth noting the bridging Ni–O–Ni angles within the cubane core, which amount to 94.6°, 97.8°, 101.6° around O2 and 95.2°, 97.6°, 101.5° around O5, respectively, for complex **1**, and amount to 94.5°, 98.6°, 100.6° around O2, 96.0°, 98.3°, 100.3° around O4, 95.3°, 98.7°, 100.3° around O6, and 95.7°, 99.9°, 97.9° around O8, respectively, for complex **2**. Figure 3 illustrates the cubane core of **1** and the binding mode of the deprotonated ligand $(L^1)^{2-}$ with the Ni^{II} ion. The ligand chelates in a nearly coplanar fashion the metal ion in an OˆNˆO coordination pocket. The alkoxy oxygen connects three adjacent Ni^{II} ions in a bridging μ_3-O binding mode, whereas the phenolate oxygen binds monodentate to a Ni^{II} ion only. In the cluster, the metal ion resides in a slightly distorted octahedral NO_5 coordination geometry, comprising oxygens from three alkoxy, one phenolate, and one ethoxy group from a ligated solvent molecule, besides one imino nitrogen. We note also that the hydroxyl hydrogen atoms of the solvent ligands form intracluster hydrogen bonds with adjacent phenolate oxygen atoms (Figure 2 and Table 3).

Table 3. Hydrogen bond distances (Å) and bond angles (°) for complexes **1** and **2**.

D–H···*A*	*d*(*D*–H)	*d*(H···*A*)	*d*(*D*···*A*)	Angle (*D*–H···*A*)
1				
O8–H8A···O6	0.93	2.66	3.462(5)	146(3)
O8–H8A···O4	0.93	2.14	2.633(4)	112(3)
O7–H7A···O3	0.93	2.64	3.377(5)	136(3)
O7–H7A···O1	0.93	1.77	2.628(4)	152(3)
2				
O12–H12···O3	0.93	1.93	2.637(6)	131(4)
O11–H11A···O1	0.93	1.72	2.594(8)	156(4)
O10–H10···O5	0.93	1.79	2.649(7)	152(4)
O9–H9···O7	0.93	1.90	2.623(7)	133(4)

Symmetry code: 1 − *x*, 2 − *y*, 1 − *z*.

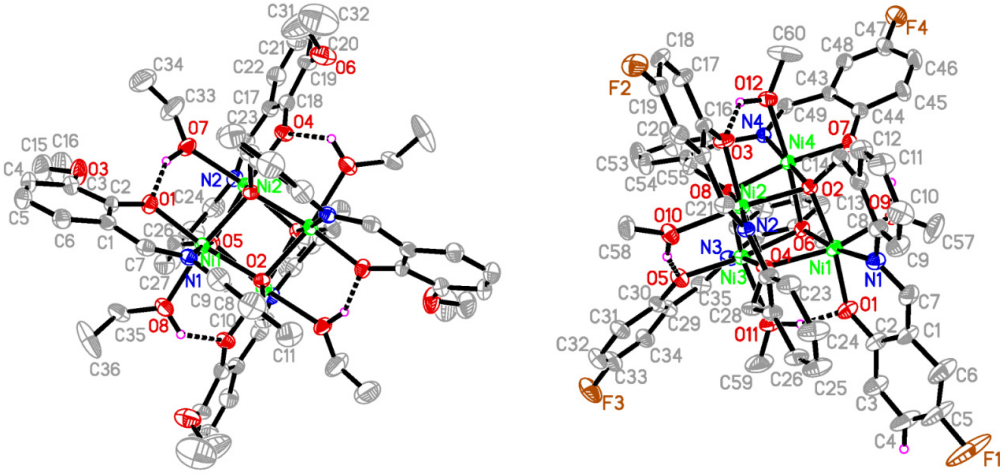

Figure 2. Crystal structures of (**a**) complex **1** (unlabeled atoms are related to the symmetry operation 1 − x, y, 3/2 − z.) and of (**b**) complex **2**. Hydrogen atoms except for those related to hydrogen bonds have been omitted for clarity. Intramolecular O–H···O hydrogen bonds are shown as dashed lines.

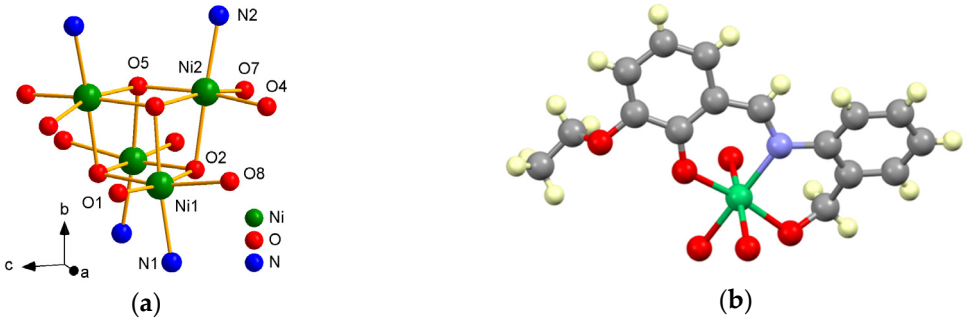

Figure 3. Cubane core (**a**) and fragment of structure **1** (**b**), emphasizing the binding mode of ligand $(L^1)^{2-}$ for Ni^{II}.

In contrast to compound **1**, there is no crystallographic two-fold rotation axis imposed on cluster **2**, which results in an additional scant variation of the structural parameters. The binding mode of $(L^2)^{2-}$ with the Ni^{II} ion for **2** is shown in Supplementary Materials Figure S1. The mean bridging Ni–O–Ni angles within the cubane core of **2** taken from all four μ_3-O atoms amount to 95.4°, 98.3°, and 100.3°, and are thus quite similar to those for **1**. The crystal packing of both compounds shows no special

feature, and due to the bulky ligand shell around the cubane core, the metal centers on neighbouring molecules are distant from each other (>8.5 Å), which minimizes any intercluster magnetic coupling.

In the crystal structure of **1** (Figure 4a), the molecules are stacked along the *b*-axis direction. In the crystal structure of **2** (Figure 4b), two adjacent molecules are linked through intermolecular C–H···F interactions, forming dimers.

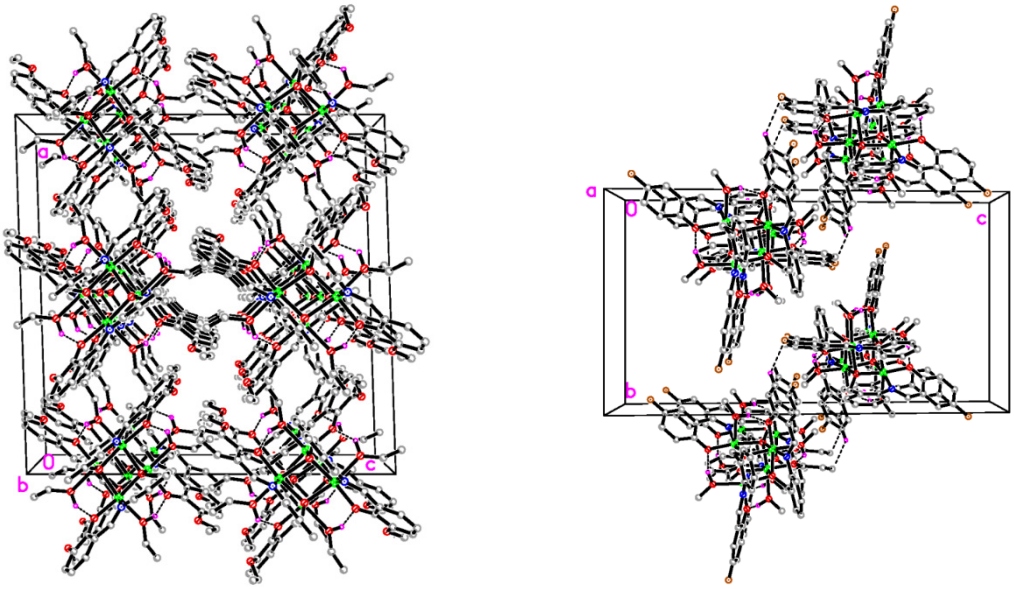

(**a**) (**b**)

Figure 4. The molecular packing diagram of complex **1** (**a**, viewed along the *b* axis) and **2** (**b**, viewed along the *a* axis). Intramolecular O–H···O hydrogen and intermolecular C–H···F interactions are shown as dashed lines.

3.3. Magnetic Properties

The temperature dependence of the magnetic susceptibilities of the complexes **1** and **2** were each measured on powder samples over the temperature range 1.9–300 K in a 1 kOe magnetic field. Transmission powder X-ray analysis was utilized to ensure that the single-crystal data were representative of the bulk material (Supplementary Materials Figure S2). At room temperature, the $\chi_M T$ product of **1** and **2** amounts to 5.9 and 5.8 cm^3 K mol^{-1}, respectively, and is thus greater than the spin-only value of 4.0 cm^3 K mol^{-1} for four noninteracting Ni^{II} ions with $S = 1$ and $g = 2$. Between 300 and 100 K, the $\chi_M T$ product for **1** and **2** increases slowly; when below 100 K the values increase more rapidly reaching a value of 17 and 24 cm^3 K mol^{-1}, respectively (Figures 5a and 6a). This increase in the $\chi_M T$ product is indicative of dominant intracube ferromagnetic interactions between the paramagnetic centers. This goes in line with the $1/\chi_M$ vs. T plot, where the data above 200 K follow the Curie–Weiss law with a positive Weiss constant θ of 7.0 and 6.8 K, respectively (Figure S3).

The field dependence of the magnetization at 1.9 K for **1** and **2** is shown in Figures 5b and 6b. The magnetization shows a rapid increase up to a field of 10 kOe, after which it increases only gradually reaching at 50 kOe values of 8.8 and 7.7 μ_B, respectively. The initial steep increase of the magnetization points as well to intramolecular ferromagnetic interactions.

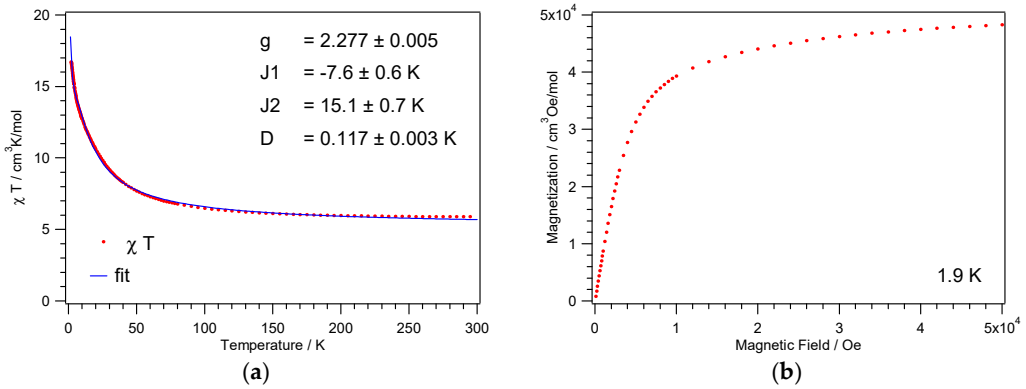

Figure 5. Temperature dependence of the $\chi_M T$ product (**a**) and magnetization vs. field (**b**) for **1**.

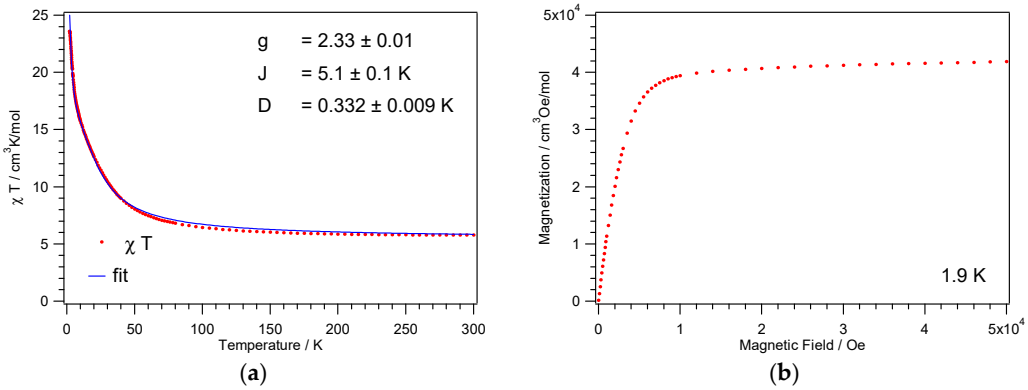

Figure 6. Temperature dependence of the $\chi_M T$ product (**a**) and magnetization vs. field (**b**) for **2**.

Given that out of the twelve Ni–O–Ni angles per cluster, eight lie in the ferromagnetic and only four in the antiferromagnetic regime, it seems useful to apply a Heisenberg Hamiltonian containing two coupling parameters, J_1 and J_2,

$$H = -2J_1(S_1S_2 + S_3S_4) - 2J_2(S_1S_3 + S_1S_4 + S_2S_3 + S_2S_4)$$

which is based on the coupling pattern as shown in Scheme 1. The Zero Field Splitting for the ground state is taken into account with the Hamiltonian

$$H = D[S_z{}^2 - S(S + 1)/3]$$

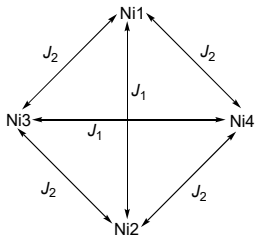

Scheme 1. Coupling scheme for **2**; for **1**, the cluster lies on a two-fold rotation axis and thus Ni2 is equivalent to Ni1 and labeled Ni1′; correspondingly, Ni3 and Ni4 are equivalent and labeled as Ni2, with Ni2′ in the structural data, see Figure 3b.

This coupling scheme with the corresponding energy levels, including Van Vlecks' equation for the magnetic susceptibility and the zero field splitting Hamiltonian, has already been described

by Escuer et al. [56]. For **1**, the best fit to the $\chi_M T$ product was achieved with parameter values for the *g*-factor $g = 2.28$, the antiferromagnetic exchange parameter $J_1 = -7.6$ K, and the ferromagnetic exchange parameter $J_2 = 15.1$ K. The resulting spin ground state, $S_T = 4$, shows a small zero field splitting $D = 0.12$ K, which is responsible for the continuous increase of the $\chi_M T$ values towards lowest temperatures, see Figure 5. The fit returns well-defined values for *g* and *D*; the parameters J_1 and J_2 are counteracting and exhibit larger error bars. The antiferromagnetic exchange J_1 is attributed to the Ni1–O2–Ni1′ and Ni2–O5–Ni2′ paths with Ni–O–Ni angles close to 101.5°, see Figure 3a and Table 2. The ferromagnetic exchange J_2 represents an average over the remaining four paths, with Ni–O–Ni angles ranging from 94° to 98°.

For the cubane core of **2**, the $\chi_M T$ fit results in $g = 2.33$, $J = 5.1$ K, and $D = 0.33$ K, see Figure 6a. As for **1**, the fit yields the spin ground state $S_T = 4$ and returns well-defined *g* and *D* parameters. However, an individual fit of J_1 and J_2 parameters was impossible. These parameters are strongly correlated, and only a single average *J* could be obtained. The cubane core of **2** exhibits no twofold rotation axis, as present in **1**. The reduced symmetry of **2** results in four individual Ni^{II} ions, see Scheme 1, and twelve different exchange paths, see Supplementary Materials Table S1. The Ni–O–Ni angles aggregate in three groups around values of 95.4°, 98.3°, and 100.3°, which is similar to **1**. Interestingly, a single ferromagnetic *J* parameter well describes the data. This *J* parameter matches well the values determined for a Ni^{II} cubane cluster with a similar Schiff-base ligand.[57] Overall, all the obtained parameters compare well with the range of parameters given in the literature for other Ni^{II} cubane clusters [56–63].

4. Conclusions

In summary, two cubane-type compounds comprising a $[Ni_4O_4]$ core and two different chelating Schiff-base ligands that offer OˆNˆO coordination pockets have been synthesized and structurally as well as magnetically characterized. Both compounds show dominant intracube ferromagnetic interactions leading to a nonzero spin ground state. It has been demonstrated that even slight structural rearrangements of the cubane core due to a different substitution pattern of the ligands lead to a noticeable variation in strengths of the magnetic coupling between Ni(II) ions. The coupling parameters, however, correlate well with the Ni–O–Ni angles determined from single crystal structure analyses.

Supplementary Materials: The following are available online at http://www.mdpi.com/2073-4352/10/7/592/s1, Figure S1: Cubane core (left) and fragment of structure **2** (right), emphasizing the binding mode of ligand $(L^2)^{2-}$ for Ni^{II}, Table S1: L-Ni-L angles (°) for complexes **1** and **2**, Supplementary Materials Figure S2: X-ray powder diffraction pattern with simulation for **1** (top) and **2** (bottom), Figure S3: The $1/\chi_M$ vs. *T* plot for **1** (left) and **2** (right).

Author Contributions: Conceptualization, Z.Y.; methodology, Y.L. (Yingying Luo), S.H., and Y.L. (Yanmin Li); investigation, Y.L. (Yingying Luo), S.H., and Y.L. (Yanmin Li); writing—original draft preparation, Z.Y., K.W.K., and S.D.; writing—review and editing, S.-X.L. and S.D.; supervision, Z.Y., K.W.K., and S.D.; project administration, Z.Y. and K.W.K. All authors have read and agreed to the published version of the manuscript.

Funding: We are grateful to the Swiss National Science Foundation for financial support under project no. 200020_172659 and the State Key Laboratory of Catalysis of China (Project No. N–19-02).

Conflicts of Interest: The authors declare no conflict of interest.

References

1. Chaudhuri, P.; Kataev, V.; Büchner, B.; Klauss, H.-H.; Kersting, B.; Meyer, F. Tetranuclear complexes in molecular magnetism: Targeted synthesis, high-field EPR and pulsed-field magnetization. *Coord. Chem. Rev.* **2009**, *253*, 2261–2285. [CrossRef]
2. Thompson, L.K. Polynuclear coordination complexes—From dinuclear to nonanuclear and beyond. *Coord. Chem. Rev.* **2002**, *233–234*, 193–206. [CrossRef]
3. Fielden, J.; Speldrich, M.; Besson, C.; Kögerler, P. Chiral hexanuclear ferric wheels. *Inorg. Chem.* **2012**, *51*, 2734–2736. [CrossRef] [PubMed]

4. Bhatt, V.; Ram, S. The role of ligands, polytopic ligands and Metal Organic Ligands (Mols) in coordination chemistry. *Chem. Sci. Rev. Lett.* **2015**, *4*, 414–428.
5. Bonanno, M.N.; Lough, J.A.; Poddutoori, K.P.; Lemaire, T.M. Synthesis, characterization and Copper(2+) coordination chemistry of a polytopic paramagnetic ligand. *Magnetochemistry* **2017**, *3*, 15. [CrossRef]
6. Winpenny, R.E.P. *Molecular Cluster Magnets*; World Scientific: London, UK, 2012.
7. Gatteschi, D. *Molecular Nanomagnets*; Oxford University Press: Oxford, UK, 2006.
8. Liu, X.; Hamon, J.-R. Recent developments in penta-, hexa- and heptadentate Schiff base ligands and their metal complexes. *Coord. Chem. Rev.* **2019**, *389*, 94–118. [CrossRef]
9. Clarke, R.M.; Herasymchuk, K.; Storr, T. Electronic structure elucidation in oxidized metal–salen complexes. *Coord. Chem. Rev.* **2017**, *352*, 67–82. [CrossRef]
10. Golcu, A.; Tumer, M.; Demirelli, H.; Wheatley, R.A. Cd(II) and Cu(II) complexes of polydentate Schiff base ligands: Synthesis, characterization, properties and biological activity. *Inorg. Chim. Acta* **2005**, *358*, 1785–1797. [CrossRef]
11. Mondal, K.C.; Kostakis, G.E.; Lan, Y.; Wernsdorfer, W.; Anson, C.E.; Powell, A.K. Defect-dicubane Ni_2Ln_2 (Ln = Dy, Tb) single molecule magnets. *Inorg. Chem.* **2011**, *50*, 11604–11611. [CrossRef]
12. Kühne, I.A.; Griffiths, K.; Hutchings, A.-J.; Townrow, O.P.E.; Eichhöfer, A.; Anson, C.E.; Kostakis, G.E.; Powell, A.K. Stepwise investigation of the influences of steric groups versus counterions to target Cu/Dy complexes. *Cryst. Growth Des.* **2017**, *17*, 5178–5190. [CrossRef]
13. Gheorghe, R.; Andreea Ionita, G.; Maxim, C.; Caneschi, A.; Sorace, L.; Andruh, M. Aggregation of heptanuclear $[M^{II}_7]$ (M = Co, Ni, Zn) clusters by a Schiff-base ligand derived from o-vanillin: Synthesis, crystal structures and magnetic properties. *Polyhedron* **2019**, *171*, 269–278. [CrossRef]
14. Wu, J.-C.; Liu, S.-X.; Keene, T.D.; Neels, A.; Mereacre, V.; Powell, A.K.; Decurtins, S. Coordination chemistry of a π-extended, rigid and redox-active tetrathiafulvalene-fused Schiff-base ligand. *Inorg. Chem.* **2008**, *47*, 3452–3459. [CrossRef] [PubMed]
15. Opstal, T.; Verpoort, F. Synthesis of highly active ruthenium indenylidene complexes for atom-transfer radical polymerization and ring-opening-metathesis polymerization. *Angew. Chem. Int. Ed.* **2003**, *42*, 2876–2879. [CrossRef] [PubMed]
16. De Clercq, B.; Verpoort, F. Atom transfer radical polymerization of vinyl monomers mediated by Schiff base ruthenium−alkylidene catalysts and the adventitious effect of water in polymerizations with the analogous cationic complexes. *Macromolecules* **2002**, *35*, 8943–8947. [CrossRef]
17. Hazra, S.; Koner, R.; Lemoine, P.; Sañudo, E.C.; Mohanta, S. Syntheses, structures and magnetic properties of heterobridged dinuclear and cubane-type tetranuclear complexes of Nickel(II) derived from a Schiff base ligand. *Eur. J. Inorg. Chem.* **2009**, *23*, 3458–3466. [CrossRef]
18. Mukherjee, P.; Drew, M.G.B.; Gómez-García, C.J.; Ghosh, A. The crucial role of polyatomic anions in molecular architecture: Structural and magnetic versatility of five Nickel(II) complexes derived from A N,N,O-Donor Schiff base ligand. *Inorg. Chem.* **2009**, *48*, 5848–5860. [CrossRef]
19. Bonadio, F.; Senna, M.-C.; Ensling, J.; Sieber, A.; Neels, A.; Stoeckli-Evans, H.; Decurtins, S. Cyano-bridged structures based on $[Mn^{II}(N_3O_2-Macrocycle)]^{2+}$: A synthetic, structural, and magnetic study. *Inorg. Chem.* **2005**, *44*, 969–978. [CrossRef]
20. Pioquinto-Mendoza, J.R.; Rosas-Ortiz, J.A.; Reyes-Martínez, R.; Conelly-Espinosa, P.; Toscano, R.A.; Germán-Acacio, J.M.; Avila-Sorrosa, A.; Baldovino-Pantaleón, O.; Morales-Morales, D. Synthesis, characterization and molecular structures of Ni(II) complexes derived from Schiff base pyridylimine ligands. *Inorg. Chim. Acta* **2015**, *438*, 146–152. [CrossRef]
21. Pioquinto-Mendoza, J.R.; Conelly-Espinosa, P.; Reyes-Martínez, R.; Toscano, R.A.; Germán-Acacio, J.M.; Avila-Sorrosa, A.; Baldovino-Pantaleón, O.; Morales-Morales, D. A simple and facile to prepare Pd(II) complex containing the pyridyl imine ligand $[C_5H_4N\text{-}2\text{-}CH_3C{=}N\text{-}(CH_2)_3NH_2]$. Structural characterization and catalytic evaluation in Suzuki–Miyaura C–C couplings. *J. Organomet. Chem.* **2015**, *797*, 153–158. [CrossRef]
22. Williams, A.F. A structural analysis of $\{M_4O_4\}$ cubanes where M = Mn and Fe. *Dalton Trans.* **2008**, *6*, 818–821. [CrossRef]
23. Isele, K.; Gigon, F.; Williams, A.F.; Bernardinelli, G.; Franz, P.; Decurtins, S. Synthesis, structure and properties of $\{M_4O_4\}$ cubanes containing nickel(ii) and cobalt(ii). *Dalton Trans.* **2007**, *3*, 332–341. [CrossRef] [PubMed]
24. Milios, C.J.; Prescimone, A.; Mishra, A.; Parsons, S.; Wernsdorfer, W.; Christou, G.; Perlepes, S.P.; Brechin, E.K. A rare ferromagnetic manganese(iii) 'cube'. *Chem. Commun.* **2007**, *2*, 153–155. [CrossRef]

25. Aronica, C.; Chumakov, Y.; Jeanneau, E.; Luneau, D.; Neugebauer, P.; Barra, A.-L.; Gillon, B.; Goujon, A.; Cousson, A.; Tercero, J.; et al. Structure, magnetic properties, polarized neutron diffraction, and theoretical study of a Copper(II) Cubane. *Chem. Eur. J.* **2008**, *14*, 9540–9548. [CrossRef] [PubMed]
26. Qin, X.; Ding, S.; Xu, X.; Wang, R.; Song, Y.; Wang, Y.; Du, C.-f.; Liu, Z.-l. Synthesis, structure and magnetic properties of a series of cubane-like clusters derived from Schiff base ligands. *Polyhedron* **2014**, *83*, 36–43. [CrossRef]
27. Isele, K.; Franz, P.; Ambrus, C.; Bernardinelli, G.; Decurtins, S.; Williams, A.F. Self-assembly and interconversion of tetranuclear Copper(II) complexes. *Inorg. Chem.* **2005**, *44*, 3896–3906. [CrossRef]
28. Papaefstathiou, G.S.; Escuer, A.; Mautner, F.A.; Raptopoulou, C.; Terzis, A.; Perlepes, S.P.; Vicente, R. Use of the Di-2−pyridyl Ketone/Acetate/Dicyanamide "Blend" in Manganese(II), Cobalt(II) and Nickel(II) Chemistry: Neutral Cubane Complexes. *Eur. J. Inorg. Chem.* **2005**, *5*, 879–893. [CrossRef]
29. Kobayashi, F.; Ohtani, R.; Teraoka, S.; Kosaka, W.; Miyasaka, H.; Zhang, Y.; Lindoy, L.F.; Hayami, S.; Nakamura, M. Syntheses, structures and magnetic properties of tetranuclear cubane-type and heptanuclear wheel-type nickel(ii) complexes with 3-methoxysalicylic acid derivatives. *Dalton Trans.* **2017**, *46*, 8555–8561. [CrossRef] [PubMed]
30. Shiga, T.; Oshio, H. Molecular cubes with high-spin ground states. *Sci. Technol. Adv. Mater* **2005**, *6*, 565–570. [CrossRef]
31. Sartorel, A.; Bonchio, M.; Campagna, S.; Scandola, F. Tetrametallic molecular catalysts for photochemical water oxidation. *Chem. Soc. Rev.* **2013**, *4*, 2262–2280. [CrossRef]
32. Song, F.; Al-Ameed, K.; Schilling, M.; Fox, T.; Luber, S.; Patzke, G.R. Mechanistically Driven Control over Cubane Oxo Cluster Catalysts. *J. Am. Chem. Soc.* **2019**, *141*, 8846–8857. [CrossRef]
33. Li, J.; Zhou, Q.; Zhong, C.; Li, S.; Shen, Z.; Pu, J.; Liu, J.; Zhou, Y.; Zhang, H.; Ma, H. $(Co/Fe)_4O_4$ cubane-containing nanorings fabricated by phosphorylating cobalt ferrite for highly efficient oxygen evolution reaction. *ACS Catal.* **2019**, *9*, 3878–3887. [CrossRef]
34. Wu, Y.-P.; Tian, J.-W.; Liu, S.; Li, B.; Zhao, J.; Ma, L.-F.; Li, D.-S.; Lan, Y.-Q.; Bu, X. Bi-Microporous metal–organic frameworks with cubane $[M_4(OH)_4]$ (M=Ni, Co) clusters and pore-space partition for electrocatalytic methanol oxidation reaction. *Angew. Chem. Int. Ed.* **2019**, *58*, 12185–12189. [CrossRef] [PubMed]
35. Yang, E.-C.; Wernsdorfer, W.; Zakharov, L.N.; Karaki, Y.; Yamaguchi, A.; Isidro, R.M.; Lu, G.-D.; Wilson, S.A.; Rheingold, A.L.; Ishimoto, H.; et al. Fast magnetization tunneling in Tetranickel(II) single-molecule magnets. *Inorg. Chem.* **2006**, *45*, 529–546. [CrossRef] [PubMed]
36. Iasco, O.; Chumakov, Y.; Guégan, F.; Gillon, B.; Lenertz, M.; Bataille, A.; Jacquot, J.-F.; Luneau, D. Mapping the magnetic anisotropy inside a Ni4 cubane spin cluster using polarized neutron diffraction. *Magnetochemistry* **2017**, *3*, 25. [CrossRef]
37. Ponomaryov, A.N.; Kim, N.; Hwang, J.; Nojiri, H.; van Tol, J.; Ozarowski, A.; Park, J.; Jang, Z.; Suh, B.; Yoon, S.; et al. Structural tailoring effects on the magnetic behavior of symmetric and asymmetric cubane-type Ni complexes. *Chem. Asian J.* **2013**, *8*, 1152–1159. [CrossRef]
38. Rudbari, H.A.; Lloret, F.; Khorshidifard, M.; Bruno, G.; Julve, M. Effects of electron donating/withdrawing groups in the 5-substituted-2−hydroxybenzaldehyde on the synthesis of neutral cubanes with a $Ni^{II}{}_4O_4$ core: Synthesis, crystal structures and magnetic properties. *RSC Adv.* **2016**, *6*, 7189–7194. [CrossRef]
39. Petit, S.; Neugebauer, P.; Pilet, G.; Chastanet, G.; Barra, A.-L.; Antunes, A.B.; Wernsdorfer, W.; Luneau, D. Condensation of a nickel tetranuclear cubane into a heptanuclear single-molecule magnet. *Inorg. Chem.* **2012**, *51*, 6645–6654. [CrossRef] [PubMed]
40. Mukherjee, S.; Weyhermüller, T.; Bothe, E.; Wieghardt, K.; Chaudhuri, P. Single-atom o-bridged urea in a Dinickel(II) complex together with $Ni^{II}{}_4$, $Cu^{II}{}_2$ and $Cu^{II}{}_4$ complexes of a pentadentate phenol-containing Schiff base with (O,N,O,N,O)-Donor atoms. *Eur. J. Inorg. Chem.* **2003**, *5*, 863–875. [CrossRef]
41. Halcrow, M.A.; Sun, J.-S.; Huffman, J.C.; Christou, G. Structural and magnetic properties of $[Ni_4(\mu_3\text{-}OMe)_4(dbm)_4(MeOH)_4]$ and $[Ni_4(\eta^1,\mu_3\text{-}N_3)_4(dbm)_4(EtOH)_4]$. Magnetostructural correlations for $[Ni_4X_4]^{4+}$ cubane complexes. *Inorg. Chem.* **1995**, *34*, 4167–4177. [CrossRef]
42. Das, A.; Klinke, F.J.; Demeshko, S.; Meyer, S.; Dechert, S.; Meyer, F. Reversible solvatomagnetic effect in novel tetranuclear cubane-type Ni4 complexes and magnetostructural correlations for the $[Ni_4(\mu_3\text{-}O)_4]$ core. *Inorg. Chem.* **2012**, *51*, 8141–8149. [CrossRef]

43. Karmakar, S.; Khanra, S. Polynuclear coordination compounds: A magnetostructural study of ferromagnetically coupled Ni_4O_4 cubane core motif. *CrystEngComm* **2014**, *16*, 2371–2383. [CrossRef]
44. Syamal, A.; Kumar, D. New oxozirconium(IV) complexes with the Schiff bases derived from salicylaldehyde or substituted salicylaldehydes and o-aminobenzyl alcohol. *Indian J. Chem. Sect. A* **1980**, *19A*, 1018–1020.
45. Syamal, A.; Singhal, O.P. New dioxouranium(VI) complexes with tridentate dibasic Schiff bases containing ONO donor sets. *Transit. Met. Chem.* **1979**, *4*, 179–182. [CrossRef]
46. Bruker. *SMART (Version 5.628) and SAINT (Version 6.02)*; Bruker AXS Inc.: Madison, WI, USA, 1998.
47. Sheldrick, G.M. *SADABS. Program for Empirical Absorption Correction of Area Detector*; University of Göttingen: Göttingen, Germany, 1996.
48. Sheldrick, G. A short history of SHELX. *Acta Crystallogr. A* **2008**, *64*, 112–122. [CrossRef]
49. Ray, A.; Sadhukhan, D.; Rosair, G.M.; Gómez-García, C.J.; Mitra, S. An unprecedented Cu^{II}–Schiff base complex existing as two different trinuclear units with strong antiferromagnetic couplings. *Polyhedron* **2009**, *28*, 3542–3550. [CrossRef]
50. Marinescu, G.; Madalan, A.M.; Shova, S.; Andruh, M. Tetranuclear Zn(II) complexes with compartmental and dicyanamido ligands: Synthesis, structure, and luminescent properties. *J. Coord. Chem.* **2012**, *65*, 1539–1547. [CrossRef]
51. Majumder, A.; Rosair, G.M.; Mallick, A.; Chattopadhyay, N.; Mitra, S. Synthesis, structures and fluorescence of nickel, zinc and cadmium complexes with the N,N,O-tridentate Schiff base N-2−pyridylmethylidene-2−hydroxy-phenylamine. *Polyhedron* **2006**, *25*, 1753–1762. [CrossRef]
52. El-Sherif, A.A.; Fetoh, A.; Abdulhamed, Y.K.; Abu El-Reash, G.M. Synthesis, structural characterization, DFT studies and biological activity of Cu(II) and Ni(II) complexes of novel hydrazone. *Inorg. Chim. Acta* **2018**, *480*, 1–15. [CrossRef]
53. Sadhukhan, D.; Ray, A.; Pilet, G.; Rizzoli, C.; Rosair, G.M.; Gómez-García, C.J.; Signorella, S.; Bellú, S.; Mitra, S. Weak interactions modulating the dimensionality in supramolecular architectures in three new Nickel(II)-hydrazone complexes, magnetostructural correlation, and catalytic potential for epoxidation of alkenes under phase transfer conditions. *Inorg. Chem.* **2011**, *50*, 8326–8339. [CrossRef]
54. Bessy Raj, B.N.; Prathapachandra Kurup, M.R.; Suresh, E. Synthesis, spectral characterization and crystal structure of N-2−hydroxy-4-methoxybenzaldehyde-N′-4-nitrobenzoyl hydrazone and its square planar Cu(II) complex. *Spectrochim. Acta A* **2008**, *71*, 1253–1260. [CrossRef]
55. Zangrando, E.; Islam, M.T.; Islam, M.A.-A.A.A.; Sheikh, M.C.; Tarafder, M.T.H.; Miyatake, R.; Zahan, R.; Hossain, M.A. Synthesis, characterization and bio-activity of nickel(II) and copper(II) complexes of a bidentate NS Schiff base of S-benzyl dithiocarbazate. *Inorg. Chim. Acta* **2015**, *427*, 278–284. [CrossRef]
56. Escuer, A.; Font-Bardıa, M.; Kumar, S.B.; Solans, X.; Vicente, R. Two new nickel(II) cubane compounds derived from pyridine-2−methoxide (Pym): $\{Ni_4(Pym)_4Cl_4(CH_3OH)_4\}$ and $\{Ni_4(Pym)_4(N_3)_4(CH_3OH)_4\}$. Crystal structures and magnetic properties. *Polyhedron* **1999**, *18*, 909–914. [CrossRef]
57. Yoshitake, M.; Nishihashi, M.; Ogata, Y.; Yoneda, K.; Yamada, Y.; Sakiyama, H.; Mishima, A.; Ohba, M.; Koikawa, M. Syntheses, structures, and magnetic properties of cubane-based cobalt and nickel complexes with ONO-tridentate ligands. *Polyhedron* **2017**, *136*, 136–142. [CrossRef]
58. Lu, Z.; Fan, T.; Guo, W.; Lu, J.; Fan, C. Synthesis, structure and magnetism of three cubane Cu(II) and Ni(II) complexes based on flexible Schiff-base ligands. *Inorg. Chim. Acta* **2013**, *400*, 191–196. [CrossRef]
59. Wikstrom, J.P.; Nazarenko, A.Y.; Reiff, W.M.; Rybak-Akimova, E.V. Synthesis and characterization of tetrakis(μ-hydroxo)tetrakis(2,2′-dipicolylamine)tetranickel perchlorate, a nickel-hydroxy cubane complex. *Inorg. Chim. Acta* **2007**, *360*, 3733–3740. [CrossRef]
60. Wang, J.; Feng, C.; Ge, C.M.; Zhang, S.; Hai, H. Two new cubane-type tetranuclear compounds of Copper(II), Nickel(II) derived from reduced schiff base ligand: Syntheses, structures and magnetic properties. *J. Clust. Sci.* **2016**, *27*, 2001–2011. [CrossRef]
61. Gungor, E.; Kara, H. Ferromagnetic coupling in two tetranuclear Ni(II) complexes with cubane–like $Ni_4(\mu_3\text{–}O)_4$ core: Structure, spectroscopic and luminescence properties. *J. Mol. Struct.* **2020**, *1208*, 127859. [CrossRef]

62. Jana, M.S.; Priego, J.L.; Jiménez-Aparicio, R.; Mondal, T.K. Novel tetranuclear Ni(II) Schiff base complex containing Ni_4O_4 cubane core: Synthesis, X-ray structure, spectra and magnetic properties. *Spectrochim. Acta A* **2014**, *133*, 714–719. [CrossRef]
63. Torić, F.; Pavlović, G.; Pajić, D.; Cindrić, M.; Zadro, K. Tetranuclear Ni_4 cubane complexes with high χT maxima: Magneto-structural analysis. *CrystEngComm* **2018**, *20*, 3917–3927. [CrossRef]